International Journal of Mass Spectrometry 300 (2011) 74–80

Contents lists available at ScienceDirect

International Journal of Mass Spectrometry

journal homepage: www.elsevier.com/locate/ijms

Strong-field ionization and dissociation studies of small early transition metal oxide clusters

Daniel E. Blumling[a,1], Scott G. Sayres[a,1], A.W. Castleman Jr.[a,b,*]

[a] Department of Chemistry, 104 Chemistry Research Building, The Pennsylvania State University, University Park, PA 16802, USA
[b] Department of Physics, 104 Chemistry Research Building, The Pennsylvania State University, University Park, PA 16802, USA

ARTICLE INFO

Article history:
Received 31 March 2010
Received in revised form 29 June 2010
Accepted 2 July 2010
Available online 17 July 2010

This paper is dedicated to John Fenn, who we acknowledge for pioneering work with molecular beams as a way of preparing and characterizing isolated clusters.

Keywords:
Coulomb explosion
Metal oxide cluster
Mass spectrometry
High charge state
Femtosecond laser
Ionization

ABSTRACT

We present the results of a systematic experimental approach utilizing time-of-flight mass spectrometry (TOF-MS) to investigate changes in maximum ionization states as the result of femtosecond pulse ionization. Strong-field gas-phase ionization experiments were performed on well characterized distributions of small early transition metal oxide (M_xO_y) clusters, where M = Ti, V, Cr, Nb, or Ta, created as a molecular beam via supersonic expansion. Utilizing high resolution TOF-MS enabled the observation of highly charged ions resulting from ionization and subsequent fragmentation via Coulomb explosion. Maximum charge states for each cluster distribution are reported as observed under various ionization conditions. Evidence for direct correlation with previously reported ionization energies of the component species is presented. Regardless of metal composition, it is observed that every cluster distribution gains approximately the same amount of energy from the external field. The extreme ionization of the targeted clusters produced ions of Ti^{10+}, V^{9+}, Cr^{8+}, Nb^{11+}, Ta^{11+}, and O^{6+}, requiring up to 216 eV of energy to create these maximum charge states via sequential ionization. Several enhanced ionization models are discussed with relation to our experimental data. Systematic investigations on the influence of cluster size and ionization laser pulse width indicate enhanced ionization contributions from the ionization ignition and charge-resonance enhanced ionization mechanisms.

1. Introduction

The strong-field enhanced ionization of clusters was first observed in the groups of Castleman [1–3] and Rhodes [4]. The mechanisms leading to enhanced ionization and subsequent Coulomb explosion in clusters have been extensively investigated for both very small (2 atoms) [5] and very large (>500 atoms) [6] systems, both theoretically and experimentally. It is established that the strong-field ionization behavior of small molecules and clusters is governed by a combination of charge-resonance enhanced ionization (CREI) [5,7], and the ionization ignition mechanism (IIM) [8] while very large systems gain energy via electron–ion interactions through the coherent electron motion [4] (CEM) model or a similar mechanism referred to as the nanoplasma model [9]. Purely metallic clusters have been demonstrated to undergo a plasmon enhanced ionization mechanism [10].

Each of these models describes the extreme ionization mechanism in clusters after the initial ionization event has occurred. The IIM model was based on a simulation from the Rose-Petruck group [8] describing the internal potential landscape formed by the attractive forces exerted by each positively charged atomic center on the surrounding electrons of the neighboring ionic cores. This attractive potential draws the valence electron density away from the parent nucleus, thus deforming the potential barrier and reducing the effective ionization potential for emission of the electrons. As more electrons are removed, the charge state of each nucleus becomes more positive and further lowers the barrier of the newly exposed electrons on neighboring nuclei. As this cycle repeats, the charges build until the cluster undergoes Coulomb explosion. IIM has been demonstrated to play a significant role in smaller noble gas, van der Waals, and hydrogen bonded clusters [2].

The generalized formulation of the dynamic CREI mechanism accounts for the oscillatory nature of the laser field. At initial cluster geometry, the internal barrier between the two nuclei is suppressed and electrons may cross freely between the potential wells. After initial ionization, the cluster begins to expand. As the separation between two ionic nuclei increases, the internal barrier between atoms also increases, thereby trapping the electrons in potential wells. However, the electric field of the laser can donate enough

* Corresponding author at: Department of Chemistry, 104 Chemistry Research Building, The Pennsylvania State University, University Park, PA 16802, USA.
Tel.: +1 814 865 7242; fax: +1 814 865 5235.
E-mail address: awc@psu.edu (A.W. Castleman Jr.).
[1] These authors contributed equally to this work.

1387-3806/$ – see front matter © 2010 Elsevier B.V. All rights reserved.
doi:10.1016/j.ijms.2010.07.002

energy to the electron to enable it to cross the inner barrier. The oscillatory nature of the laser field directs the electrons to repeatedly cross the barrier, thus increasing their energy simultaneously with the rising of the barrier. At a critical separation, (R_c), the electron motion can become resonant with the laser frequency leading to a large enhancement in the energy absorption cross-section. Eventually the electrons gain enough energy to surpass the outer barrier, and ionize. Finally, as the internuclear distance grows beyond R_c, the internal barrier rises above the energy provided by the external field and the enhanced ionization process ceases [7]. Theoretical work performed by Rost and coworkers has increased understanding of the CREI mechanism in small clusters. Their studies on rare-gas clusters composed of 16–30 atoms [11] led to the important conclusion that CREI is manifested most significantly in small clusters. This mechanism is not a collective behavior, but instead a cooperative effect between two ions. The presence of an additional layer of atoms beyond the two aligned properly for the ionization enhancement would retard the outer ionization of any released electrons [12]. This mechanism has been used to explain results in heterocyclic molecules [13], as well as and HI-Ar van der Waals clusters [7].

The CEM model was originally developed to explain the production of X-rays observed in large clusters being subjected to intense laser radiation [4]. This mechanism relies predominantly on the effects of collectively oscillating electrons. Following initial ionization, the freed electrons and ionic cores are treated as quasi-particles remaining within the influence of the external driving field. As this field oscillates, the electrons gain energy, which is then donated to the cluster via inelastic electron scattering, similar to electron impact, heating the cluster and leading to further ionization. This mechanism has also been determined to contribute to the ionization of methyl iodide clusters [14,15].

The nanoplasma model is similar in mechanism to CEM, where the dominant energy absorption process is through inelastic electron collisions, but here inverse bremsstrahlung heating also becomes important. A key difference is the continued emission of X-rays from the cluster after the laser pulse has passed due to the slower cooling rate of the plasma with respect to the expansion of the cluster [9]. With the formation of the plasma, the expansion of the cluster is now dominated by the hydrodynamic pressure of the electrons. This nanoplasma model applies to clusters containing thousands of atoms. In that size regime, the cluster is treated as a dielectric sphere and exhibits an enhanced absorption of energy when the electron density reaches a critical value which brings the plasma frequency into resonance with the external field.

Meiwes-Broer et al. introduced a plasmon enhanced ionization mechanism [10] to explain the results of their work on small homogenous metal (Pb, Pt, and Ag) clusters [16–18] where expansion is dominated by Coulomb forces. This model is restricted to purely metallic systems, which exhibit plasmonic behavior even at low energies due to electron delocalization. An enhancement in energy absorption is expected when the plasmon energy of the metal cluster becomes resonant with the photon energy of the light. Plasmon enhanced ionization is an extension of the more general models of, CEM and CREI, as it requires both collective electron effects and a resonance with the electric field.

However, despite the development of several models and theoretical treatments, experimental investigations into the ionization behavior and explosion dynamics of small clusters (3–50 atoms) have been limited. The nanoplasma model is ignored in this discussion, as it requires very large clusters which are absent here. Therefore, in order to further expand our understanding regarding the role of IIM, CREI, and CEM ionization mechanisms as they pertain to our current studies, we have conducted extensive new investigations of these processes.

As noted above, past studies of small clusters have been largely focused on those species homogeneously composed of metals, rare-gas atoms, or molecules. In contrast, the clusters studied in this work consisted of binary component systems. The transition metal oxide complexes possess significantly polar covalent bonding in which the strong electronegativity of the oxygen species creates a heterogeneous electron distribution between an oxygen atom and a neighboring metal nucleus [19]. These clusters represent a previously unexplored realm of molecular/cluster interaction with strong fields.

2. Experimental methods

Strong-field ionization studies were performed on small transition metal oxide clusters using a time-of-flight mass spectrometer (TOF-MS). This technique is highly successful in the determination of the identities of multiply-charged ions [20] as ion flight times are proportional to their mass to charge ratios. From the mass spectra, and associated arrival times, the maximum observed charge state (MOCS) for each element of the target cluster, and the kinetic energy released (KER) from the subsequent Coulomb explosion of the highly charged ions was measured. Relative values for this energy were calculated using the observed peak splitting between forward and backward ejected ionic species [13].

Our sample preparation technique relies heavily on the pioneering work of John Fenn regarding the use of molecular beams as a way of preparing and characterizing isolated clusters [21]. Here, clusters were created in a laser ablation source by desorbing transition metal from the surface of a pure metal rod (species used in these studies were Ti, V, Cr, Nb, and Ta; 99% purity) by means of a focused nanosecond Nd:YAG laser operating at 10 Hz. The intensity of the laser was varied for each metal species and was adjusted prior to each experiment to ensure maximum cluster production within the chosen size regime. Concomitantly with the ablation event, a 300 μs duration pulse of oxygen gas seeded in helium was released from a pulsed valve outlet and directed over the ablation site. The resulting plasma of metal, oxygen, and helium atoms then interacted within a small "waiting room" before completing their clustering and cooling during a supersonic expansion into the vacuum chamber (1×10^{-6} Torr). By utilizing subtle changes in the ablation laser fluence, gas concentrations and pressures, as well as the expansion nozzle length and waiting room geometry, the relative distribution of cluster sizes were controlled and systematically shifted towards smaller or larger clusters.

The resulting cluster beam contained both neutral and ionic species which were then skimmed via a 5 mm conical orifice prior to entering the laser–cluster interaction region located between the first two plates of a two-stage Wiley–McLaren [22] style TOF-MS extraction region. These two ion optics were maintained at static high positive voltages, serving to direct the resulting ions from the ionization event downstream into the TOF-MS, which was oriented normal to the direction of the molecular beam. In addition, the static field deflected any ionic cluster species in the beam, allowing only neutral clusters to enter the ionization region. Ionization was induced via pulses of 624 nm light provided by a previously described [23] amplified colliding pulse, mode-locked (CPM) dye laser, also operating at 10 Hz. Amplification was attained via a Bowtie amplifier and three Bethune cell amplifiers, each pumped by the second harmonic of a 10 Hz nanosecond Nd:YAG laser. Prior to entering the cluster interaction region, the linearly polarized laser beam was focused by a 50 cm focusing lens to provide intensities of approximately 1×10^{15} W/cm^2. Typical pulse durations were 100 fs and pulse stretching to 350 fs was accomplished by removal of two recompression gratings in the beam path (both pulse trains were characterized via an autocorrelation technique).

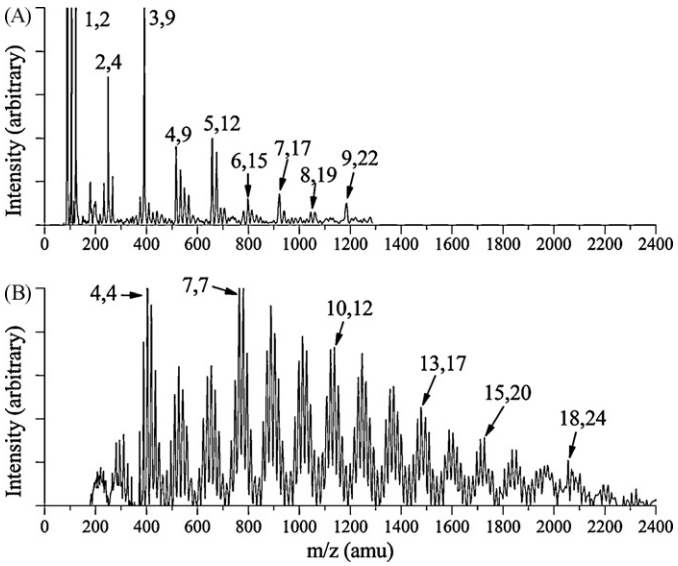

Fig. 1. Mass spectra of neutral niobium oxide clusters present in two selectively controlled molecular beams. These species were identified in the time-of-flight mass spectrometer following single ionization via our defocused femtosecond laser. The values provided are in the format (x, y) for the species Nb_xO_y. (A) Contains a typical mass spectrum of smaller niobium oxide clusters used in this work. The heavier distribution shown in (B) results from subtle source modifications, as described in the text, and defines the distribution of clusters utilized in the experiments described in Section 3.2.2.

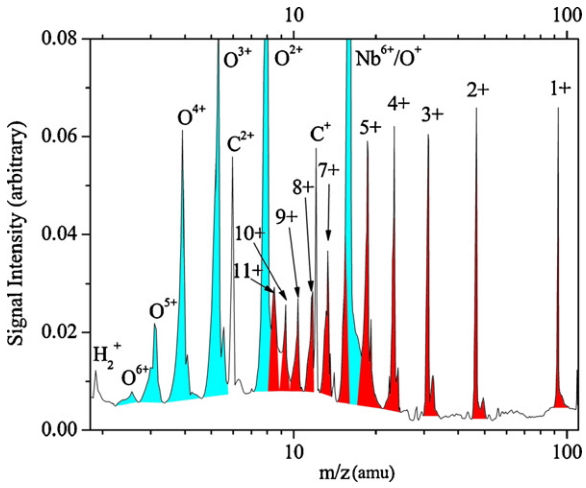

Fig. 2. Mass spectrum of the multiply-charged ions produced by strong-field ionization via the intense (1×10^{15} W/cm^2) femtosecond pulse of 100 fs in duration. The m/z ratio axis is plotted logarithmically for clarity. Charge states for the metal species are provided without an elemental designation for clarity. MOCS values for the resulting ions of the target Nb_xO_y cluster are Nb^{11+} and O^{6+}.

Following irradiation, the cationic products were accelerated into the TOF-MS wherein they encountered two beam steering devices, a three-stage Einzel lens and a two element deflector plate assembly. As noted above, MOCS and KER values were recorded independently. To obtain clear peak splittings which allowed for the calculation of KER values for each ionic species, a linear field-free region of 1.3 m was utilized in conjunction with a microchannel plate (MCP) detector. This approach yielded a large signal intensity without the use of the Einzel lens, which could have influenced the KER measurements. For our observations of maximum charge states for the various ionic species, a reflectron was utilized in "hard-reflection" mode to extent the length of the field-free region to approximately 2.5 m. This aided in resolving the otherwise narrow distribution of multiply-charged ionic species. Here, ion detection was also performed with a MCP detector. Both detectors were coupled with an oscilloscope used in conjunction with a personal computer for data analysis.

3. Results and discussion

Mass spectra of the neutral cluster species present in these experiments were obtained by defocusing the femtosecond laser beam to minimize the strong-field effects and allow the clusters to become singly ionized with minimum fragmentation. This allowed for the initial identification of neutral cluster species, thereby affording the ability to easily shift the focal point to provide the intensities which are required for strong-field ionization without changing any other experimental parameters. A typical mass spectrum following the single ionization of neutral niobium oxide clusters via the defocused beam is provided in Fig. 1.

As evidenced in the mass spectrum, the observable distribution of species ranges from the niobium monomer up to clusters containing a total of 31 (niobium + oxygen) atoms. This approach to ionizing the neutral cluster species for identification yielded a highly reliable and useful depiction of the species present in the molecular beam. However, this technique cannot ensure that the ionizing femtosecond laser is not distorting the observed distribution through fragmentation of larger clusters. To alleviate this concern, cationic and anionic cluster mass spectra were also obtained, and the sizes observed in those distributions were well correlated to the neutral species. To examine the ionic clusters, the time-of-flight grids were initially grounded and then pulsed to high voltages as the clusters arrived in the extraction region. The ion distributions were obtained without use of the femtosecond laser, as the species were already ionized. This procedure was performed for each of the target cluster species, each containing oxygen clustered to a different transition metal (Ti, V, Cr, Nb, and Ta) and the conditions of the laser ablation source were easily controlled to yield similar distributions regardless of constituent metal. These distributions were kept small (fewer than 40 total atoms) with clusters containing 12–18 atoms often being the most intense species in the spectra.

3.1. Maximum observed charge states (MOCS)

Following neutral cluster ionization and identification, the ionizing laser was tightly focused on the target clusters, attaining energy densities on the order of 10^{15} W/cm^2. Multiple ionization events resulted from the high intensity of the incident laser and mass spectra were recorded to identify the product ions. Fig. 2 contains a typical spectrum resulting from the strong-field ionization of the niobium oxide cluster distribution shown in Fig. 1A.

Note that the maximum charge state observed for the niobium species is the Nb^{11+} ion and the counterpart oxygen species are observed to only reach the O^{6+} state. In these experiments, the carbon species are a contamination due to vaporized hydrocarbon-based pump oil used in our vacuum systems. The hydrogen dimer most likely results from the ionization/dissociation of water. Strong-field ionization experiments were performed on each cluster system and the resulting MOCS value for each constituent atom within those clusters was identified (see Table 1). These extreme levels of ionization are attained via enhanced ionization phenom-

Table 1
MOCS values for each of the component atomic nuclei composing the target cluster species.

Species	Ti_xO_y	V_xO_y	Cr_xO_y	Nb_xO_y	Ta_xO_y
Metal	10	9	8	11	11
Oxygen	6	6	6	6	6

Table 2
IE energies from the available literature [27] and estimated using Slater's Rules (in parentheses). The MOCS for each species is denoted in bold. The 9th ionization energy for chromium is marked with a dagger to indicate that although it was not observed in our experiments due to mass degeneracies, its presence is expected (see text for details). All values are provided in electron volts (eV).

Ionization state	Oxygen	Titanium	Vanadium	Chromium	Niobium	Tantalum
1	13.6 (14.2)	6.8 (7.5)	6.8 (8.4)	6.7 (9.3)	6.8 (7.2)	7.5 (6.5)
2	35.1 (33.3)	13.6 (12.2)	14.6 (13.2)	16.5 (14.3)	14 (11.3)	(10.3)
3	54.9 (55)	27.5 (16.1)	29.3 (18.5)	30.9 (20.8)	25.0 (12.2)	(10.4)
4	77.4 (79.2)	43.3 (24.2)	46.7 (27.6)	49.2 (30.9)	38.3 (18.1)	(15.5)
5	113.9 (105.8)	99.3 (93.8)	65.3 (37.8)	69.5 (42.1)	50.6 (24.9)	(21.2)
6	**138.1 (135)**	119.5 (114.7)	128.1 (120.4)	90.6 (54.4)	102.1 (109.1)	(113.8)
7	739.3 (742.6)	140.8 (136.7)	150.6 (143.4)	160.2 (150)	(126.3)	(132.6)
8	871.4 (870.8)	170.4 (159.8)	173.4 (167.5)	184.7 (175.1)	(144.3)	(152)
9	–	192.1 (184)	**205.8 (192.8)**	**209 (201.4)**†	(163)	(172.2)
10	–	**215.9 (209.4)**	230.5 (219.1)	244.4 (228.7)	(182.4)	(193.1)
11	–	265.1 (235.8)	255.7 (246.6)	270.8 (257.2)	**(202.5)**	**(214.8)**
12	–	291.5 (263.4)	308.1 (275.1)	298 (286.8)	(223.4)	(237.2)

ena which result from the interactions between the clusters and the strong external field.

Typical femtosecond laser parameters provided intensities of approximately 1×10^{15} W/cm^2 at the focal point of the beam. Using the relation $U_p = 9.33 \times 10^{-14} I\lambda^2$, where I is the intensity of the laser at its focus (in W/cm^2) and λ is the central wavelength of the incident radiation (in micrometers) we can obtain the ponderomotive potential (U_p, in eV), associated with the laser pulse. Using the above intensity and the CPM laser's central wavelength of 624 nm, U_p is calculated to be approximately 36.3 eV. Field ionization alone would be insufficient to remove more than the first three electrons from any of the transition metal species studied in these experiments. An electron ejected from a cluster with a linearly polarized laser pulse can have a maximum recoil energy of $3.17U_p$ [24], which in this case is 115 eV. This allows ionization up to the valence shell closing for most atoms, but not beyond. Therefore, the clustered nature of the target systems is influencing the ionization behavior observed in these experiments.

As laser intensities increase, photoexcitation behaviors lose their multiphoton character and tunnel ionization processes can significantly contribute to the electron dynamics. The barrier at which this transition occurs is conventionally approximated using the Keldysh, or adiabatic, parameter (γ) which is determined using the equation $\gamma = (\mathrm{IP}/2U_p)^{1/2}$ [25]. This simple approximation is based on the ionization potential (IP) of the target species and the ponderomotive potential of the incident electric field calculated above. In this relationship, if $\gamma \gg 1$ then ionization is dominated by multiphoton ionization while values of $\gamma \ll 1$ indicate a greater contribution by tunnel ionization. Using the first IP of atomic niobium (6.5 eV) this equation yields a Keldysh parameter of ~0.3 and the first IP of atomic oxygen (13.62 eV) results in a value of ~0.43. Both values identify electron tunneling as the dominant ionization mechanism for the removal of even the first electron from each species.

Based on the results shown in Table 1, there are several trends which deserve further discussion. The first trend in maximum charge states is manifested in the cluster species containing Row IV transition metals. The maximum charge states observed for the transition metal species steadily decrease with a corresponding increase in atomic mass. However, the oxygen species for each cluster series result in identical maximum charge states of O^{6+}. Previous research has suggested that after the initial bonding electrons are removed, an atomic response is expected from the core electrons [26]. Therefore, reported atomic ionization energies lend insight into this behavior serving as a valid template for comparing the relative amounts of energy gained by the target systems. Ignoring the specific perturbations created by the ionization enhancement mechanisms, the unperturbed ionization potentials represent the total amount of energy which must be absorbed by a system to ionize an electron, whether that energy is donated via internal interactions or the external field.

The atomic IE values available from the literature [27] for each of the three Row IV metal species are listed in Table 2. The first several ionization energies for each species are quite similar. The large jump in ionization energy for each species (5th for Ti, 6th for V, and 7th for Cr) indicates the complete removal of all 3d and 4s valence electrons and the stripping of the first 3p electron from the atom. Initial inspection of the MOCS shows that the energy required to sequentially ionize the 10th electron from a Ti^{9+} ion is approximately 216 eV while the energies required to create V^{9+} and Cr^{8+} are approximately 206 eV and 185 eV, respectively. The appearance of each of these three species demonstrates that, regardless of the transition metal component, approximately the same amount of energy is gained by each cluster. The clear absence of the Ti^{11+} ion (or any higher charge states of the other species) is demonstrative of the fact that the most energy which can be donated to clusters of this size, under our specific laser conditions, is somewhat less than 265 eV of energy, a value which is required for the creation of Ti^{11+}. Thus in the absence of observable V^{10+} ions the ionization dynamics within the clusters do not allow the creation of ions requiring more than 230 eV of energy. Specifically, each atom in the cluster gains more than 185 eV, but less than 230 eV, through interaction with the strong field of the laser prior to explosive fragmentation.

The absence of the Cr^{9+} ion (5.77 amu) is the result of its relative mass degeneracy with the C^{2+} (6.0055 amu) ion. This mass degeneracy is further obscured by the inherent peak splitting associated with the kinetic energy release associated with the Coulomb explosion event. However, its creation is expected based on the reported ionization energies. Approximately 209 eV is required to remove the 9th electron from a chromium atom, which is slightly less than that required for the observed Ti^{10+} charge state. The production of O^{6+} ions in each experiment and the overall absence of the O^{7+} species follow according to the behaviors detailed above. The ionization energy required for O^{6+} is approximately 138 eV which is significantly less than the energy needed to create the maximum metal charge states. Meanwhile, the IE for O^{7+} (the creation of which represents the removal of a 1s electron) requires approximately 739.3 eV of energy, well beyond the limit of absorption expected for these studies. Thus, the sequential ionization energies of each transition metal species in Row IV (and their counterpart oxygen atoms) can be directly related to the MOCS for each species.

As depicted in Table 2, the ionization energy trend for increasingly higher charge states of niobium follows the same pattern as that observed (and previously discussed above) for the vanadium series. This is due to the similarities in their shell closings and electronic orbital characteristics. It is notable, however, that

each reported energy for the niobium charge state is significantly lower than its vanadium counterpart. Again, this is easily attributed to their electronic structures. The valence electrons of niobium are less tightly bound to the nucleus of their parent atoms due to their increased distance (and increased interelectronic shielding) from the atom's core. Thus, it is not surprising that the MOCS value observed for the niobium oxide cluster distribution is higher than that of the vanadium series. In the truncated literature data available, the Nb^{7+} ion requires a nearly degenerate amount of ionization energy as the V^{6+} ion, a trend that should clearly continue as additional electrons are removed.

In the absence of sufficient literature values for the niobium and tantalum series, we have approximated the energies required for sequential ionization using Slater's rules [28]. These values have been provided in Table 2 next to their corresponding literature values, where applicable. As shown, these calculations are in relatively good agreement with the literature values, especially at the higher ionization energies. According to our calculations, creation of the Nb^{11+} ion requires approximately 203 eV of energy while the Ta^{11+} charge state requires 214.8 eV. These values are fully consistent with the previous observation that the targeted clusters gain at least 185 eV, but not more than 230 eV of energy during the enhanced ionization processes regardless of their constituent species.

3.2. Origin of the enhanced ionization behavior

As noted above, the highly charged ions resulting from the strong-field irradiation of the target clusters are not originating from field ionization alone, as the ponderomotive potential of the field is insufficient in magnitude. We now examine other enhancement mechanisms to explain the extreme ionization observed.

3.2.1. Ionization pulse width experiments

It has been demonstrated that the CEM mechanism is sensitive to changes in excitation pulse width. In the event that CEM is providing significant enhancement to the ionization, increasing the pulse width will allow any field-driven electrons to inelastically scatter with the cluster over a longer period of time, leading to increased heating and additional enhanced ionization. This effect was clearly demonstrated in homonuclear metal clusters composed of 20–100 atoms by the Meiwes-Broer group who reported observations of Pt^{5+} following irradiation with a 140fs pulse but Pt^{9+} ion production with a 290 fs pulse using 800 nm light [29]. To determine the effect of CEM on the clusters studied here, we have adjusted the laser optics used in the creation and amplification of our laser pulse train to lengthen each pulse from 100 fs to approximately 350 fs, as described in the above experimental section. The overall power was maintained at a constant 1.5 mJ to provide consistency between the experiments. However, it should be noted that as the pulse width is lengthened by a factor of 3.5, the peak laser intensity drops by the same factor.

The results of pulse width dependency experiments on our small clusters of Nb_xO_y clusters are shown in Fig. 3. The MOCS values for the experiment were Nb^{11+} and O^{6+} in both the long- and short-pulse environments. The significantly lower population of the more highly charged species (Nb^{6+} through Nb^{10+}) is due to the significant increase in energy (~51.5 eV) required to remove the first core electron (the 6th overall electron, and the first from the 4p shell) from the niobium atom. Despite a threefold increase in the ionization pulse width, it is clear from Fig. 3 that the relative distributions of the observed ionic species are comparable and that there is no observable change in the MOCS. However, the data suggests there may be a very small shift in the distribution to more highly ionized species as a result of the longer excitation pulse width. This indicates that the mechanism(s) responsible for enhanced ionization

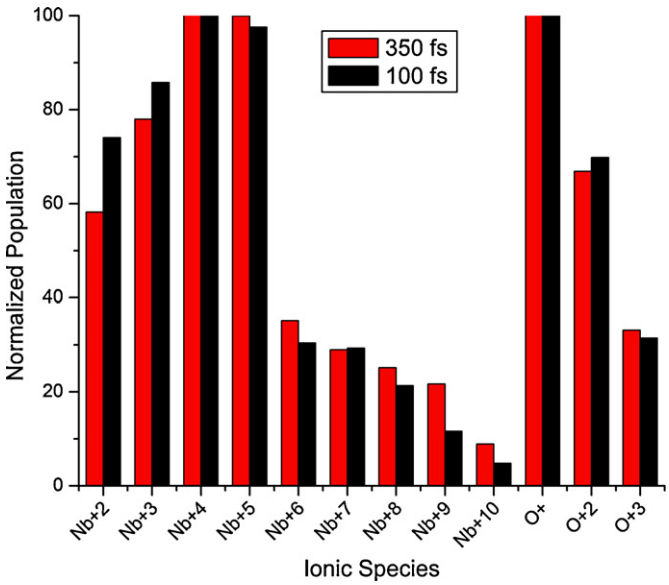

Fig. 3. Normalized ion populations for the multiply charged species resulting from strong-field ionization via a 350 fs pulse and a 100 fs pulse of small niobium oxide clusters. The signal from the Nb^{11+} ion in each distribution was excluded due to insufficient signal for accurate comparison and Nb^{+} was omitted because of irresolvable convolution of the multiphoton ionized atomic species in the cluster distribution and those resulting from the strong-field ionization and fragmentation of clusters. Each set of data is normalized to the most intense peak in the spectrum.

may have a slight dependence on the change in pulse width for the systems studied here.

Comparison of the kinetic energy release measurements for both pulse widths of light indicates that our targeted systems reached the maximum states at different ionization rates. The more gradual leading edge of the 350 fs pulse resulted in a slower rate of energy absorption for each charged species than that observed with the 100 fs pulse. This allows the repulsive forces between neighboring ions to expand the cluster further prior to ionization resulting in lower Coulomb explosion KER values. Data for several charge states of both the niobium and oxygen ions are provided and demonstrate clear differences in the measured KER for each species. These species in particular were chosen because their kinetic energy splitting in the mass signal was well resolved within the same potential gradient in the extraction region of the mass spectrometer. The presented data clearly demonstrates the increased expansion of the clusters during longer excitation pulses, yet there was no evidence of enhancement (or degradation) in the maximum ionization state of the atoms within the cluster, proving that ionization is not necessarily a vertical process. The results of these measurements are shown in Fig. 4.

3.2.2. Enhanced ionization dependency on cluster size

The systems described herein are too small to allow for any significant contributions from electron impact [30], as the mean free path of the electron is much larger than the collisional cross-section of clusters this size. Smaller clusters, such as those with structures calculated by Zhai et al. [31] and Fielicke et al. [32] generally posses only one "layer" of atoms with respect to the cluster's center, in a cage-like formation. The effect of the shift to larger clusters is manifested in the formation of a second "shell" of atoms extending from the center of the cluster. The multi-shell nature of larger clusters may prove to be pivotal in allowing CEM to occur, as this mechanism is strongly dependant on the size of the cluster. To confirm this idea, ionization pulse width studies were also performed on cluster distributions containing significantly larger species.

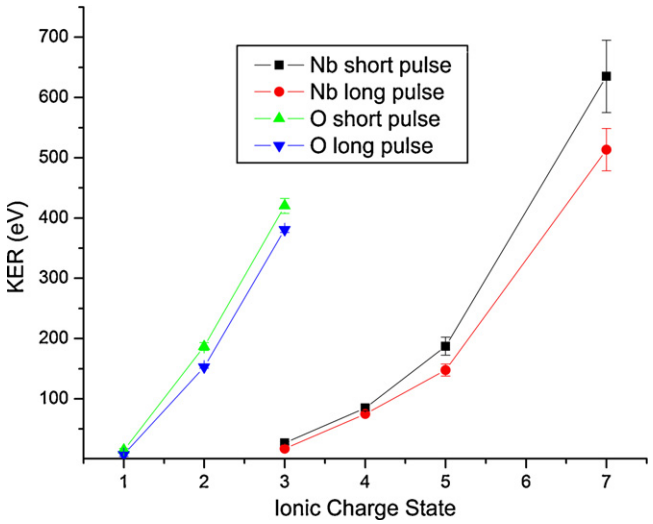

Fig. 4. KER values for selected niobium and oxygen atoms to demonstrate cluster expansion during both long (350 fs) and short (100 fs) ionization pulses. Nb^{6+} was omitted due to its similar m/z ratio with the large signal from the O^+ ion (see Fig. 2). Similarly, O^{4+} was not included due to its mass degeneracy with background signal from C^{3+}. Further mass degeneracy issues precluded the accurate analysis of higher charge states for each species.

Fig. 1B contains a mass spectrum of the niobium oxide cluster distribution created upon changing our source conditions to preferentially form heavier clusters. In Fig. 1A, the lighter cluster distribution is dominated by clusters composed of approximately 11 atoms while the heavier distribution contains significant populations of clusters composed of up to 35 atoms. The heavy distribution contains species with an average of 20 atoms, but remains fairly uniform in contributions from various clusters throughout the spectrum. Following both 100 fs and 350 fs wide laser pulse ionization of this heavier distribution, we again observed MOCS values of Nb^{11+} and O^{6+}, which are identical to those attained from the small cluster studies. Based on our observations, it is clear that there are no significant collective electron effects participating in the ionization enhancement of our irradiated cluster systems.

Despite our experimental similarities to previously published work [16], i.e., similar cluster size (~20 atoms vs. ~22 atoms, on average), similar wavelength (624 nm vs. 800 nm), and similar pulse width change (100–350 fs vs. 140–450 fs), we did not observe any further ionization beyond the Nb^{11+} or O^{6+} charge states, regardless of ionization laser pulse width. To explain this behavior, we focus on the fundamental differences between previously reported work and the clusters currently under investigation. The lack of collective electron effects is attributed to the heteronuclear nature of our clusters. Aside from the initial differences in electronegativity between two different adjacent atoms within our clusters, the situation is further complicated due to the various ionization potentials for each atomic species, leading to varying charge states within the cluster and manifesting as a dynamically changing intercluster potential landscape. An inhomogeneous field, such as that expected from the multiple ionization of our heteronuclear clusters, likely fails to provide an ideal environment for CEM, as there would be ionic "hot-spots" throughout the cluster whenever the constituent atoms were ionized to differing charge states, therefore further suppressing CEM effects.

Additionally, the ionic-covalent bonds present in the transition metal oxide clusters lead to faster expansion rates. The metal oxide bonds are shorter (~2 Å) than the internuclear distances associated with the metallic bonding of pure metal clusters (~3 Å) causing the initial Coulomb repulsion between ions to be stronger. The oxygen atoms are located on the exterior of the cluster, typically forming either dangling or bridging bonds [33]. Due to their position and mass, they obtain proportionally larger amounts of KE during repulsion based on Coulomb's law. Following the initial tunneling ionization, these lighter ions are highly repulsed by the heavy transition metal ions in the core of the cluster, leading to a rapid expansion of the cluster's outermost atoms. Thus, the distance dependent effects from CREI are still viable. However, the cluster density decreases rapidly, minimizing the electron scattering cross-section for heating via CEM.

While the average number of constituent atoms per cluster in our experiments was comparable to those reported by Meiwes-Broer and coworkers, the maximum reported cluster sizes differ significantly. We did not observe the presence of clusters containing more than 40 atoms within our distributions, whereas the studies on pure metal clusters reported the production of clusters containing a maximum of ~100 atoms. The coherent electron motion ionization enhancement reported in those studies may be due to dynamics which only manifest in the largest species of the distribution and thus would not be observable in the smaller clusters studied here. Finally, the fact that the clusters studied here are not purely metallic further eliminates the possibility of significant plasmon enhanced ionization.

The extreme ionization phenomena observed in this work is likely due to a combination of the IIM and CREI. The relatively short bonds found between the atoms in our metal oxide clusters allow the effects of IIM to be much more prominent, as the force between charged species decreases quadratically with distance according to Coulomb's law. Additionally, the ionization potentials of the metal and oxygen are not the same, leading to an even more pronounced inhomogeneous internal electric field as ionization progresses. The positive charges of the ions perturb the electrons of the neighboring nuclei, and in conjunction with field-dressing of the electrons, the ionization energies associated with valence and even core electrons are sufficiently suppressed that ionization proceeds. We observe little dependence on cluster size to the distribution of charge states, in accordance with IIM.

The CREI mechanism has been determined in the past to influence the enhanced ionization in small clusters [11]. Our results from the pulse width experiments demonstrate that the ions are not completely frozen during the ionization process, thus ionization is not vertical and occurs concomitantly with the expansion. As the cluster loses the first few electrons, its constituent atoms begins to separate allowing the electron's energy levels to come into resonance with the laser field amplifying the energy absorption. The longer pulse width resulted in a slower expansion, and therefore a longer resonance time was achieved. This led to the small shift towards higher charge state in the overall distribution. The mechanism benefits from the rapid expansion of low mass ions, increasing the probability that the internuclear distances reach r_c. Through the presence of additional shells, the outer nuclei of larger clusters can confine an ionized electron within the dimensions of the cluster itself, preventing outer ionization [12]. We suggest the absence of multiple shells in our cluster distribution and the presence of cage-like structures provide an excellent platform for the CREI mechanism.

Theoretical work regarding strong-field ionization of heterogeneous clusters is limited due to the intense computational workload inherent in dealing with complex multi-electron dynamics which occur in polyatomic systems. To further complicate the matter, the ionization rates of transition metal atoms are notoriously difficult to determine, as the multiple delocalized valence electrons associated with transition metals prohibit the use of a single active electron approximations [34]. Significant screening can occur as the incident electric field polarizes the atom and increases the potential barrier retarding the ejection of valence electrons and thus lowers the field ionization rate [34].

4. Conclusions

In conclusion, strong-field ($I \sim 10^{15}$ W/cm^2) ionization experiments were performed on small transition metal (Ti, V, Cr, Nb, or Ta) oxide clusters which yielded a variety of maximum charge states. The MOCS values were explained using the periodic trends in ionization energies associated with the correlating atomic species. All of the observed charge states extended well beyond expected values based on simple field ionization of the atomic species. Enhanced ionization occurs within the cluster as a function of the superposition of the external electric field and the internal potential landscape of the cluster itself. Tunneling ionization leads to the initial removal of electrons within the cluster, creating an inhomogeneous potential gradient within the clusters.

An increase in maximum charge state as a function of increasing atomic mass was observed for the Group Vb experiments while lower maximum charge states for increasing mass was seen for the Row IV species. These findings were rationalized using literature IP values and approximations attained using Slater's rules. It was determined that the charge states created for each species corresponded to the absorption of nearly identical amounts of energy due to the laser–cluster interactions, regardless of the transition metal species, suggesting that the extent of ionization is dependent on the threshold for sequential ionization.

Further, experiments investigating the effects of pulse width on niobium oxide clusters of two different mass ranges were performed to qualify the ionization enhancement phenomena which contributed to the creation of our highly charged ions. Despite significant systematic changes to the cluster size, there were no changes in the maximum observed charge states. Only a small shift in the high charge state distribution was observed for an increase in laser pulse width. As the CEM mechanism is strongly dependent upon both of these variables, our results indicate that this is not the mechanism of the ionization enhancement within the clusters studied. However, the shift in distribution is consistent with CREI. Hence, we conclude that both IIM and CREI mechanisms are responsible for the ionization enhancement in small transition metal oxide clusters.

Acknowledgement

We acknowledge support from the Department of Energy, grant # DE-FG02-92ER-14258.

References

[1] J. Purnell, E.M. Snyder, S. Wei, A.W. Castleman Jr., Chem. Phys. Lett. 229 (1994) 333.
[2] E.M. Snyder, S.A. Buzza, A.W. Castleman Jr., Phys. Rev. Lett. 77 (1996) 3347.
[3] E.M. Snyder, S. Wei, J. Purnell, S.A. Buzza, A.W. Castleman Jr., Chem. Phys. Lett. 248 (1996) 1.
[4] A. Mcpherson, B.D. Thompson, A.B. Borisov, K. Boyer, C.K. Rhodes, Nature 370 (1994) 631.
[5] T. Zuo, A.D. Bandrauk, Phys. Rev. A 52 (1995) R2511.
[6] I. Last, J. Jortner, Phys. Rev. A 62 (2000) 013201.
[7] I. Last, J. Jortner, Phys. Rev. A 58 (1998) 3826.
[8] C. Rose-Petruck, K.J. Schafer, K.R. Wilson, C.P.J. Barty, Phys. Rev. A 55 (1997) 1182.
[9] T. Ditmire, T. Donnelly, A.M. Rubenchik, R.W. Falcone, M.D. Perry, Phys. Rev. A 53 (1996) 3379.
[10] L. Köller, M. Schumacher, J. Köhn, S. Teuber, J. Tiggesbäumker, K.H. Meiwes-Broer, Phys. Rev. Lett. 82 (1999) 3783.
[11] C. Siedschlag, J.M. Rost, Phys. Rev. A 67 (2003) 013404.
[12] U. Saalmann, C. Siedschlag, J.M. Rost, J. Phys. B: At. Mol. Opt. Phys. 39 (2006) R39.
[13] D.A. Card, E.S. Wisniewski, D.E. Folmer, A.W. Castleman Jr., J. Chem. Phys. 116 (2002) 3554.
[14] J.V. Ford, L. Poth, Q. Zhong, A.W. Castleman Jr., Int. J. Mass Spectrosc. 192 (1999) 327.
[15] J.V. Ford, Q. Zhong, L. Poth, A.W. Castleman Jr., J. Chem. Phys. 110 (1999) 6257.
[16] M. Schumacher, S. Teuber, L. Köller, J. Köhn, J. Tiggesbäumker, K.H. Meiwes-Broer, Eur. Phys. J. D 9 (1999) 411.
[17] T. Döppner, T. Fennel, T. Diederich, J. Tiggesbäumker, K.H. Meiwes-Broer, Phys. Rev. Lett. 94 (2005) 013401.
[18] T. Döppner, S. Teuber, M. Schumacher, J. Tiggesbäumker, K.H. Meiwes-Broer, Int. J. Mass Spectrom. 192 (1999) 387.
[19] G.E. Johnson, R. Mitrić, M. Nössler, E.C. Tyo, V. Bonačić-Koutecký, A.W. Castleman Jr., J. Am. Chem. Soc. 131 (2009) 5460.
[20] M. Mann, C.K. Meng, J.B. Fenn, Anal. Chem. 61 (1989) 1702.
[21] J.B. Anderson, J.B. Fenn, Phys. Fluids 8 (1965) 780.
[22] W. Wiley, I. McLaren, Rev. Sci. Instrum. 26 (1955) 1150.
[23] S. Wei, J. Purnell, S.A. Buzza, R.J. Stanley, A.W. Castleman Jr., J. Chem. Phys. 97 (1992) 9480.
[24] P.B. Corkum, Phys. Rev. Lett. 71 (1993) 1994.
[25] L.V. Keldysh, Sov. Phys. JETP 20 (1964) 1307.
[26] S. Palaniyappan, R. Mitchell, R. Sauer, I. Ghebregziabher, S.L. White, M.F. Decamp, B.C. Walker, Phys. Rev. Lett. 100 (2008) 183001.
[27] D.R. Lide (Ed.), CRC Handbook of Chemistry and Physics, 90th ed. (Internet Version 2010), CRC Press/Taylor and Francis, Boca Raton, FL, 2010.
[28] J.C. Slater, Phys. Rev. 36 (1930) 57.
[29] P. Radcliffe, T. Döppner, M. Schumacher, S. Teuber, J. Tiggesbäumker, K.H. Meiwes-Broer, Contrib. Plasma Phys. 45 (2005) 424.
[30] K. Ishikawa, T. Blenski, Phys. Rev. A 62 (2000) 063204.
[31] H.J. Zhai, J. Döebler, J. Sauer, L.S. Wang, J. Am. Chem. Soc. 129 (2007) 13270.
[32] A. Fielicke, G. Meijer, G. von Helden, J. Am. Chem. Soc. 125 (2003) 3659.
[33] D.R. Justes, R. Mitrić, N.A. Moore, V. Bonačić-Koutecký, A.W. Castleman Jr., J. Am. Chem. Soc. 125 (2003) 6289.
[34] M. Smits, C.A. de Lange, A. Stolow, D.M. Rayner, Phys. Rev. Lett. 93 (2004) 203402.